



U.S. Department of Energy
Oakland Operations Office, Oakland, California 94612

Lawrence Livermore National Laboratory
University of California, Livermore, California 94551



UCRL-ID-144879

Field Measurements of Electro-osmotic Transport of Ground Water Contaminants in a Lithologically Heterogeneous Alluvial-Fan Setting

Authors

**W. W. McNab, Jr.
J. A. Karachewski*
G. S. Weissmann****

Contributors

**R. Depue
K. Heyward**

July 2001

*Weiss Associates, Emeryville, California

**Department of Geological Sciences, Michigan State University, East Lansing, Michigan



Environmental Protection Department
Environmental Restoration Program and Division

DISCLAIMER

This document was prepared as an account of work sponsored by an agency of the United States Government. Neither the United States Government nor the University of California nor any of their employees, makes any warranty, express or implied, or assumes any legal liability or responsibility for the accuracy, completeness, or usefulness of any information, apparatus, product, or process disclosed, or represents that its use would not infringe privately owned rights. Reference herein to any specific commercial product, process, or service by trade name, trademark, manufacturer, or otherwise, does not necessarily constitute or imply its endorsement, recommendation, or favoring by the United States Government or the University of California. The views and opinions of authors expressed herein do not necessarily state or reflect those of the United States Government or the University of California, and shall not be used for advertising or product endorsement purposes.

This work was performed under the auspices of the U. S. Department of Energy by the University of California, Lawrence Livermore National Laboratory under Contract No. W-7405-Eng-48.

This report has been reproduced
directly from the best available copy.

Available to DOE and DOE contractors from the
Office of Scientific and Technical Information
P.O. Box 62, Oak Ridge, TN 37831
Prices available from (423) 576-8401
<http://apollo.osti.gov/bridge/>

Available to the public from the
National Technical Information Service
U.S. Department of Commerce
5285 Port Royal Rd.,
Springfield, VA 22161
<http://www.ntis.gov/>

OR

Lawrence Livermore National Laboratory
Technical Information Department's Digital Library
<http://www.llnl.gov/tid/Library.html>

Field Measurements of Electro-osmotic Transport of Ground Water Contaminants in a Lithologically Heterogeneous Alluvial-Fan Setting

Authors

**W. W. McNab, Jr.
J. A. Karachewski*
G. S. Weissmann****

Contributors

**R. Depue
K. Heyward**

July 2001

*Weiss Associates, Emeryville, California

**Department of Geological Sciences, Michigan State University, East Lansing, Michigan

**Environmental Protection Department
Environmental Restoration Division**

Table of Contents

1. Introduction.....	1
1.1. Site Description and History.....	2
1.1.1. Wellfield.....	2
1.1.2. Hydrogeologic and Lithologic Characterization.....	2
1.1.3. Implications for EO Operations.....	4
1.1.4. Distribution of Contaminants.....	4
1.2. Electro-osmosis System.....	5
1.2.1. Design.....	5
1.2.2. Results of Initial Operations.....	5
1.3. EO System Modeling.....	7
1.4. Discussion.....	9
2. Acknowledgments.....	9
3. References.....	10

List of Figures

- Figure 1. Aerial photograph of LLNL Livermore site.
- Figure 2. An east-west oriented cross section along the southern boundary of the EO deployment site.
- Figure 3. Photograph of a typical gravel hydrofacies sample.
- Figure 4. Photograph of a typical sand hydrofacies sample.
- Figure 5. Photograph of a typical sandy silt hydrofacies sample.
- Figure 6. Photograph of a typical paleosol hydrofacies sample.
- Figure 7. Isopach map of lowest channel deposit within HSU 3A.
- Figure 8a. Sediment total chlorinated hydrocarbon concentrations, grouped by lithologies as delineated by lithologic description of continuous cores.
- Figure 8b. Sediment total chlorinated hydrocarbon concentrations, grouped by lithologies as delineated by geophysical logs.
- Figure 9. EO system layout: schematic (top) and photograph of Helipad EO deployment site (bottom).
- Figure 10. Cathode membrane assembly.

- Figure 11. Chlorinated hydrocarbon concentration histories (concentrations normalized to those measured at the commencement of sampling) for wells W-1552, W-1651, and W-1654.
- Figure 12. An idealized mixed tank model of pump-and-treat with re-injection in Helipad area wells.
- Figure 13. Normalized concentration histories as interpolated by the mixed tank model for wells W-1552, W-1651, and W-1654.
- Figure 14a. Normalized concentration histories of TCE in well W-1552 and carbon tetrachloride in well W-1654.
- Figure 14b. Estimated $\Delta c/\Delta t$ values, corrected by the mixed tank interpolation model.
- Figure 15. A comparison of frequency distributions of corrected $\Delta c/\Delta t$ values under EO and non-EO operating conditions.

List of Tables

- Table 1. $\Delta c/\Delta t$ values for key chlorinated hydrocarbon compounds in each of the three extraction/cathode wells.

List of Attachments

- Attachment A. Electro-osmosis Screening Model.....A-1
- Attachment B. Pumping Model in 3-D.....B-1

1. Introduction

Remediation of contaminated ground water by pump-and-treat approaches is often problematic because the heterogeneous distributions of lithologies, and hence hydraulic conductivities, characterizing many aquifers result in complex flow paths. Consequently, contaminants are removed readily from the most permeable regions of the subsurface but the less permeable sediments, rich in clay and silt, remain largely undisturbed. These continue to act as diffusion-limited sources for further contamination of the permeable sediments. Under certain circumstances, specialized technologies, such as electrokinetic approaches, may be useful for enhancing the removal of ground water from low-permeability sediments. These circumstances generally include high contaminant concentrations — hence posing a chronic source threat — and a relatively small area requiring treatment. At Lawrence Livermore National Laboratory (LLNL) in Livermore, California, electro-osmosis (EO) is being evaluated as a means for extracting ground water containing trichloroethylene (TCE) and other chlorinated hydrocarbons from fine-grained sediments in a plume source area.

EO was first applied to de-water clay for soil stabilization projects (e.g., Casagrande, 1952). In recent years, the potential of using EO for removing contaminants from fine-grained sediments has been explored in both laboratory studies and field-scale demonstrations (Hamed et al., 1991; Bruell et al., 1992; Segall and Bruell, 1992; Acar and Alshwabkeh, 1993; Lageman, 1993; Probstein and Hicks, 1993; Shapiro et al., 1993). Recently, the DOE-funded Lasagna™ Project at the Paducah Gaseous Diffusion Plant employed electro-osmosis to transport TCE to activated carbon or iron filing treatment zones within the electric field, resulting in an estimated removal efficiency ranging from 95% to over 99% (Ho et al., 1999a,b). With regard to the LLNL Livermore Site in particular, previous bench-top tests using representative samples demonstrated that EO can increase the effective hydraulic conductivity of fine-grained sediments by two orders-of-magnitude (Pico, 2000; Cherepy et al., 1999).

Briefly, EO entails the movement of pore water under the influence of an electric field, as opposed to that under a hydraulic gradient (Mitchell, 1993). This movement is a result of the coulomb attraction of the diffusive double layer (the cloud of water molecules and positively-charged ions that forms over the negatively-charged surfaces of clay minerals) from the anode toward the cathode. Viscous drag tends to pull the remaining pore water in the same direction. The flux of water associated with EO, q , is proportional to the voltage gradient, $\nabla\phi$,

$$q = \frac{-k_{eo}}{n} \nabla\phi \quad (1)$$

where k_{eo} is the electro-osmotic conductivity and n the porosity. In principle, the electro-osmotic conductivity is not a true constant of the material because it depends on a number of factors (e.g., ζ -potential) which may vary with pH and other variables. However, the k_{eo} is nonetheless useful for engineering design purposes (Mitchell, 1993).

Because the source sediments at the LLNL demonstration site exhibit heterogeneous lithologies, electro-osmotic treatment of fine-grained sediments is being coupled directly with pump-and-treat

extraction of ground water from coarse-grained sediments. This remediation strategy presents challenges in interpreting the effects of EO on contaminant transport because of the difficulty in separating the electro-osmotic and Darcian flux components within the same well field (McNab and Ruiz, 2001). This study presents a means for separating the two flux components based on the integration of lithologic data, initial contaminant distributions between lithologies, modeling, and statistical analyses of contaminant fluxes to the extraction wells. The methodology is developed not only to assist in interpreting the system performance but also to assist in validating generalized models of electro-osmotic flow through sediments.

1.1. Site Description and History

LLNL is located along the southeastern margin of the fault-bounded Livermore Valley of the California Coast Ranges, approximately 55 kilometers east of San Francisco. LLNL is underlain by a thick sequence of unconsolidated Quaternary alluvial-fan deposits, informally referred to as the Livermore Gravels. Previous investigators (Blake et al., 1995; Noyes et al., 2000) integrated geologic, analytical, ground water elevation, and hydraulic test data to identify eight hydrostratigraphic units (HSUs) that control ground water flow and contaminant transport within the aquifer beneath LLNL.

Chlorinated hydrocarbons (primarily TCE and tetrachloroethylene [PCE]) are in ground water at LLNL as a result of past disposal practices by LLNL and the U.S. Navy, the prior steward of the property. This EO field-scale demonstration was located in the Helipad Area within the northeastern portion of LLNL (Figure 1). This area is also located downgradient from a former landfill that operated from the mid-1950s until about 1970. Although the sediment and debris in the former landfill were excavated in 1984, subsequent investigations confirmed that the subsurface in the vicinity of the former landfill was contaminated with high concentrations of chlorinated hydrocarbons (CVOCs) in both sediment (up to 315 $\mu\text{g}/\text{kg}$) and ground water (up to 10,081 $\mu\text{g}/\text{L}$).

1.1.1. Wellfield

The EO system in the Helipad area incorporated nine wells arranged in a square array and spaced approximately 25 feet (8 m) apart (Figure 1). All nine wells were screened within HSUs 3A and 3B, approximately 100 to 130 (30.5 to 39.6 m) feet below ground, because this interval contained relatively high concentrations of chlorinated hydrocarbons and generally fine-grained sediments (Figure 2). Anodes were installed in six wells: three wells along the western perimeter and three wells along the eastern perimeter. The anode wells were also used for ground water reinjection of treated water during operation of the EO system. Cathodes were installed in three wells within the center of the array. The cathode wells were also used for ground water extraction during EO operations.

1.1.2. Hydrogeologic and Lithologic Characterization

Lithologic characterization is an essential element in assessing the applicability and the effectiveness of an EO system. The lateral continuity of fine-grained sediments and their contaminant distribution become key issues for understanding EO flow. In contrast, the coarse-grained sediments control hydraulic flow during concurrent ground water extraction and injection operations. To assess the lithologic heterogeneity and distribution of both fine-grained and coarse-

grained sediments, continuous cores were collected from five of nine borings drilled at the site. The cores were described for textural and sedimentologic characteristics including visual estimation of grain size, grain shape, grain sorting, and color, as well as sedimentary and pedogenic (soil) structures. In addition, geophysical logs were obtained from each well and were used for correlation of hydrofacies on cross sections. Based on these descriptions, four hydrofacies dominate the section. These include gravel and sand hydrofacies of channel deposits, sandy silt hydrofacies of overbank deposits, and paleosol hydrofacies that represent extended periods of sediment exposure to soil formation (Gile et al., 1979; Gile et al., 1981).

Gravel hydrofacies. The gravel hydrofacies is dominated by clast-supported gravel, pebbles, and cobbles that are typically weathered and held in a reddish, clay-rich matrix (Figure 3). These deposits tend to be massive at the scale of the core. Clay coats on clasts appear to be oriented parallel to clast surfaces, thus indicating possible pedogenic or secondary origin of the clays. Additionally, manganese (Mn) oxides are common on the clay coatings, indicating alternating wetting and drying of the sediment consistent with pedogenic alteration in the present and probable past climates of the site – e.g., Mediterranean climate during interglacial periods and wetter climate, as found in northern California, during glacial periods (Kolterman and Gorelick, 1992). Though this hydrofacies tends to display the highest hydraulic conductivity of the section, the presence of thick clay coats on all grains probably significantly reduces the hydraulic conductivity from that expected of more typical gravelly deposits. On geophysical logs, the gravel hydrofacies character is readily distinguished by relatively high resistivity and relatively low gamma ray signatures.

Sand hydrofacies. The sand hydrofacies typically consists of well to moderately well sorted fine to medium sand with some zones containing coarse to very coarse sand (Figure 4). The sandy deposits are generally massive to vaguely cross-stratified, and grains are typically subrounded. In some units, the clays coat the sand grains indicating some degree of pedogenic alteration. On geophysical logs, the sand hydrofacies character is distinguished by relatively high resistivity, typically a bit lower than that of the gravel hydrofacies, and relatively low gamma ray signatures.

Sandy silt hydrofacies. The sandy silt hydrofacies typically consists of silt that contains fine to medium sand. The sandy silt hydrofacies typically displays some evidence of pedogenic alteration, including the presence of root traces that are commonly clay-filled and show reduction halos, thin clay coats on ped faces, dispersed Mn-oxides, and brown coloration (Figure 5). These sediments were most likely deposited on floodplains of the Livermore alluvial fans. On geophysical logs, the sandy silt hydrofacies character is distinguished by relatively low resistivity and relatively high gamma ray signatures.

Paleosol hydrofacies. The paleosol hydrofacies typically consists of sandy clay-rich deposits that display evidence of significant pedogenic alteration (Figure 6). Evidence for pedogenic alteration includes very thick clay coats on ped faces, continuous Mn-oxide coats on ped faces, slightly prismatic to prismatic or blocky structure, occasional root traces, and, in most cases, reddening. Additionally, many paleosols contain significant calcium carbonate indicating a relatively dry climate during paleosol development. On geophysical logs, the paleosol hydrofacies character is difficult to distinguish from the sandy silt hydrofacies since it, too, displays low resistivity and high gamma ray, however some paleosol units display slightly higher gamma ray response due to the higher clay content.

1.1.3. Implications for EO Operations

The only facies that can be correlated between most wells with any degree of confidence is the paleosol hydrofacies. These units appear to be laterally extensive, and when missing in wells, the predicted paleosol location contains gravel or sand, indicating that a channel most likely eroded the paleosol from that location. These paleosols delineate important stratigraphic boundaries in the LLNL alluvial-fan system and correlate with previously defined HSU boundaries. Based on these correlations, the paleosols and fine-grained floodplain deposits (sandy silt) may control compartmentalization of the aquifer system. Caution should be exercised when using this interpretation, however, since breaks in the paleosols may make them ineffective barriers to flow.

Characterization of the core also indicated that high clay contents exist in paleosols and in pore spaces of gravels, with lesser amounts of clay in floodplain sandy silts and channel sands. These distributions of clay will probably control the effectiveness of EO remediation and should be considered when modeling this system.

Since the EO deployment focused on remediation of contaminants in HSUs 3A and 3B, isopach maps of the sand bodies within these units were also constructed. The channels in these units are generally oriented from south to north (Figure 7). In general, the sands are thicker and more common toward the western and central part of the study area. Greater hydraulic communication was noted between the western line of anode wells and the central line of cathode wells (Figure 2) most likely due to channel deposits controlling local ground water flow.

1.1.4. Distribution of Contaminants

During drilling of the EO wells, sediment samples were collected from continuous cores in each hydrofacies every one to two feet (30 to 60 cm) for chemical analysis (Method 601). The highest concentrations of chlorinated hydrocarbons were detected in HSUs 3A and 3B within the southern and central part of the area, with the maximum concentration of 315 µg/kg being detected in well W-1653. In contrast, the concentrations of total chlorinated hydrocarbons were less than 140 mg/kg in the northern three wells.

The distributions of contaminant concentrations among sediment types is of obvious relevance to the long-term efficacy of EO system operations, and, in the short term, also holds consequences for interpreting initial system performance. A comparison of contaminant concentration versus lithology is presented in Figure 8a, and a similar comparison between contaminant concentration and geophysical log signature is presented in Figure 8b. Both figures show that fine-grained sediments contain higher contaminant concentrations in the Helipad area than the more permeable sands and gravels. It is plausible that lower contaminant concentrations in the sand and gravel hydrofacies may be, in part, a result of a sampling bias associated with flushing of these more permeable sediments by drilling mud during recovery of the core.

The ground water in the EO wells also showed higher concentrations of chlorinated hydrocarbons in the southern and central parts of the area. Prior to the start of pump-and-treat operations in the fall of 1999, the maximum concentration of total chlorinated hydrocarbons was 10,081 µg/L in well W-1552. The primary contaminant of concern was TCE, although PCE, 1,1-dichloroethylene (DCE), 1,2-dichloroethane (DCA), and carbon tetrachloride were detected at concentrations at least two orders of magnitude above their Maximum Contaminant Levels. Since October 2000, the concentrations of chlorinated hydrocarbons in ground water have decreased and

become more uniform in all the wells due to combined EO and pump-and-treat operations and injection of treated ground water into the anode wells.

1.2. Electro-osmosis System

1.2.1. Design

The EO system is shown on Figure 9. Contaminated ground water is drawn to the three central cathode/extraction wells by both EO flow and hydraulic pumping. Sustainable pumping rates for all three of the cathode wells are generally less than approximately 0.5 gal/min. During the initial phases of operation, electric current was limited to approximately 6 amps per cathode, corresponding to a total voltage drop between the cathode and anode electrodes of approximately 80 V.

Water is circulated between the electrodes and buffering tanks at the surface to maintain pH neutrality in the face of electrolysis reactions at both types of electrodes. pH control is necessary to prevent the acidification of the sediments near the anodes (with a consequent reduction in electro-osmotic conductivity of the sediment) as well as formation of mineral deposits (carbonates and metal hydroxides) at the cathodes under alkaline conditions. For the cathode wells, the water-recirculation system entailed installing an ion-permeable membrane assembly around each electrode to facilitate water management (Figure 10). In addition to helping manage pH control, the membrane assembly/recirculation system provides a means for venting H₂ gas generated by electrolysis as well as a means for radiating excess heat (denoted as “*q*” on Figure 10).

Extracted ground water is treated in a portable treatment unit (PTU) that removes chlorinated hydrocarbons by air-stripping with activated carbon adsorption. Treated water is returned to the subsurface by injection at the anode wells to facilitate water management. Support equipment includes submersible pumps, water level sensors, and flow meters for each well, along with a manifold assembly that directs the flow of water between the extraction wells, the pH adjustment units for the cathode and anode arrays, the water treatment facility, and the injection wells. Computerized data acquisition and automated safety interlock systems permits operation of the treatment system (both EO and pump-and-treat components) on a 24-hr/7-day basis.

1.2.2. Results of Initial Operations

The pump-and-treat components of the treatment system were operated on near-continuous basis from October 2000 through February 2001 (the system did not operate for a two-week period during the winter holidays). The EO component of the treatment system operated intermittently during the time period, amassing a total operating period of approximately 300 hours. Much of the down time associated with the EO component of the system was the result of debugging new equipment, modifying procedures, and by several mechanical failures of the cathode membrane assemblies. These difficulties are currently being addressed through modifications to the system design.

The multiple start and stop sequences of the EO system operation offered the opportunity to compare system performance with and without EO while the pump-and-treat with re-injection system continued operations. Because the concentrations of chlorinated hydrocarbons in fine-grained sediments in the Helipad Area apparently exceed those in the coarse-grained materials,

differences in contaminant influxes to the three extraction/cathode wells between periods of EO system operation and non-operation offered a chance of observing EO effects directly. This is because operation of the EO system, even during relatively short time intervals (on the order of a few days) should draw some contaminant-enriched ground water out of fine-grained materials in the immediate vicinity of the extraction well bores (where voltage gradients are highest). An increase in contaminant influx to the extraction wells is detectable in principle using statistical techniques to compare concentrations in samples collected from the extraction wells during operations both with and without EO.

Chemical concentration trends for the three chlorinated hydrocarbons detected most frequently in the Helipad area – TCE, carbon tetrachloride, and chloroform – are depicted on Figure 11; concentrations are normalized for each compound by its respective initial concentration. A decline in concentration with time is clearly evident for each compound in each well. It is quite plausible that much of this trend is associated with the reinjection scheme that serves to dilute the contamination. An idealized mixed tank model (Figure 12) provides a means for interpolating the concentration trends based on this mechanism (Figure 13).

If the overall downward concentration trends in the Helipad Area are a result of pump-and-treat with re-injection (or, at least, may be interpolated in a satisfactory way by the model), then the scatter about the trends shown on Figure 13 may, in part, reflect the sporadic starting and stopping of the EO system. To test this hypothesis, changes in normalized concentration per unit time were corrected for the effects of pump-and-treat dilution by the following equation:

$$\frac{\Delta c_i}{\Delta t} = \frac{c_i + c_{i-1}(1 - e^{-\lambda \Delta t}) - c_{i-1}}{\Delta t} \quad (2)$$

An example of application of equation 2 to historical concentration trends is illustrated on Figure 14a and b. Once the long-term historical trend is removed (which would impart a consistent negative trend for $\Delta c/\Delta t$ values), the individual $\Delta c/\Delta t$ spikes that occur from one sampling event to the next become evident. The key to identifying evidence of an EO response is to check for any correlations between the occurrences or magnitudes of spikes and instances when EO operations were underway (indicating by shading on the Figure 14b).

Values for $\Delta c/\Delta t$, calculated via equation 2, for all three compounds of interest from all three extraction/cathode wells are listed on Table 1; values are given in percentages since concentrations are normalized as described previously. Conditions under which samples were collected (EO or non-EO) are indicated on the table. The two sample populations (EO and non-EO) were used to

generate frequency distribution histograms (Figure 15). Inspection of the histograms indicates a tendency for positive corrected $\Delta c/\Delta t$ values (average = + 2.4%/day; median = +2.3%/day) during EO operations and essentially no central tendency (average = -0.3%/day; median = -0.2%/day) when the EO system was not operating. Among all the data points, a tendency for positive $\Delta c/\Delta t$ spikes during EO operations, and no tendency (i.e., an equal likelihood of negative or positive $\Delta c/\Delta t$ spikes) during non-EO operations provides a statistical basis supporting that a response from the system to EO had been observed. A rank-sum statistical test confirmed the significance of the difference between the two distributions ($\alpha < 0.001$, or confidence level $> 99.9\%$). In other words, a comparison of the two data sets collected under EO and non-EO conditions, respectively, while pump-and-treat continued to operate strongly suggests a measurable increase in contaminant influxes to the extraction wells (on the order of 2%/day). The implication of the rank-sum test result is that the probability that this difference is due simply to random chance is very low.

1.3. EO System Modeling

The comparative analysis of contaminant removal rates during periods with and without operation of the EO system provides an indication that induced electro-osmotic fluxes exert a measurable effect on system performance. However, the question of the overall benefit to aquifer remediation in terms of reduced operating time in the targeted area requires further analysis. In calculating electro-osmotically induced fluxes, consider the following relationships:

- A point source solution to the steady-state potential field problem, integrated in the vertical direction to simulate a line source (i.e., an electrode), to predict the potential (i.e., voltage), ϕ , as a function of position with respect to the line source, can provide a simplified model of the voltage distribution about the electrode array:

$$\phi(x, y, z) = \sum_{j=1}^N \frac{1}{L} \int_{ze_j}^{ze_j+L} \frac{I_j}{4\pi\sigma_s} \left(\frac{1}{r_e} - \frac{1}{\sqrt{(x-xe_j)^2 + (y-ye_j)^2 + (z-\xi)^2}} \right) d\xi \quad (3)$$

where L is the electrode length, σ_s the electrical conductivity of the soil, xe_j , ye_j , and ze_j , the coordinates for the location of the bottom of each electrode, and r_e the electrode radius. Superposition, indicated by the summation, allows for multiple electrodes, N , with the sign on the current flow through each j th electrode, I_j , used to distinguish anodes and cathodes. Thus, equation 3 accepts current flow through individual electrodes as input and can be used to calculate the voltage difference between electrodes.

- An estimate of sediment electro-osmotic conductivity, k_{eo} (derived from previous measurements or estimated from literature values), taken with the electrode geometry, electric current, and an estimated σ_s , can be used to estimate the electro-osmotically induced velocity vector at any location in the electrode array field. Because the electro-osmotic flux is, as an engineering approximation, proportional to the voltage gradient (equation 1), the local ground water velocity components due strictly to EO are given by,

$$v = \begin{bmatrix} -\frac{k_{eo}}{n} \frac{\partial \phi}{\partial x} \\ -\frac{k_{eo}}{n} \frac{\partial \phi}{\partial y} \\ -\frac{k_{eo}}{n} \frac{\partial \phi}{\partial z} \end{bmatrix} \quad (4)$$

where n is the material porosity and the voltage gradient components are calculated by numerical differentiation of equation 3 (assuming k_{eo} is not directionally dependent).

- With the relationship given in equation 4 available for quantifying the EO-induced flow field, the calculated summation of the EO fluxes across a mathematical cylindrical surface surrounding an electrode provides an approximation of the flux of water, Q , to the well (neglecting contributions across the top and the base of the cylinder),

$$Q = L \int_0^{2\pi} n v_n \left(x e + \rho \cos(\theta), y e + \rho \sin(\theta), z e + \frac{L}{2} \right) \rho d\theta \quad (5)$$

where v_n is the component of the EO-induced ground water velocity vector normal to the cylinder at the midpoint of its length (L), ρ the radius of the cylinder, and θ the variable of integration.

Utilizing MathCad 8.0 (MathSoft, Inc.) as a computational platform, a semi-analytical model of electro-osmotic transport was developed (see Attachment A) based upon previously measured values of σ_s and k_{eo} in LLNL soils. Given the specifications of the EO array at the Helipad site and the magnitudes of the electrical currents supplied, the induced water flux under initial operating conditions to each electrode would be expected to be on the order of about 15–20 cc/min, or an increase of approximately 1% over hydraulic pumping rates. Assuming that contaminant concentrations within the fine-grained materials exceed those in more permeable materials by a factor of 5–10 and that fine-grained materials constitute at least half of the lithologic column encountered by the electrodes at the Helipad site (see discussions earlier in this report), then the observed increases in contaminant influxes to the extraction wells during EO operations (~2%/day) are quantitatively consistent with expectation.

The semi-analytical model can readily be extended to forecast system performance in terms of long-term. In particular, particle tracking may be employed to calculate travel time from a point within the electrode array to the nearest cathode well under electro-osmotic migration. This travel time may then be compared to a similar calculation involving hydraulic pumping in fine-grained material. Using the MathCad model presented in Attachment A, travel times were calculated for a particle initially positioned at the center of a hypothetical 2×2 anode-cathode electrode set, with well geometries, sediment properties, and operating constraints approximately reflective of conditions at the Helipad site. For comparison, an analogous calculation was performed to assess the rate at which hydraulic pumping could transport a contaminant from the same origin to an extraction well functioning at the cathode location (Attachment B). For this calculation, Darcy's

law is substituted for Ohm's law, so that electric current is replaced by water flux, voltage potential by hydraulic head, and electrical conductivity by hydraulic conductivity. Hence, each cathode or anode well becomes a hydraulic injection or extraction well, respectively. The model assumed a hydraulic conductivity of 1×10^{-7} cm/s, essentially representing a silt lithology.

In an idealized, homogeneous lithologic domain, the prescribed low hydraulic conductivity implies that the maximum extraction rate that could be achieved would be limited to a value on the order of 0.001 gal/day; higher pumping rates would require head gradients between extraction and injection wells that could not be achieved, given the available drawdown. As a result, particle travel time from the origin point to the nearest extraction well is approximately 150 years. In contrast, the calculated travel time for the comparable EO system, operating at 6 amps per cathode, is approximately 32 years. If electric current were increased to 20 amps, which should be achievable using the current system configuration with modifications to the pH control system, travel time would be reduced to approximately 10 years.

1.4. Discussion

The travel time estimates for both pump-and-treat and EO are based upon idealized models that assume a homogeneous lithology characterized by uniform values of hydraulic conductivity and electro-osmotic conductivity. In reality, of course, heterogeneities in the subsurface will result in preferential flow pathways for ground water, and to a much lesser extent, electric current and electro-osmotic fluxes. Without very detailed characterization of the spatial variabilities in hydraulic conductivity, electro-osmotic conductivity, and electrical conductivity of the sediments (the latter two attributes varying somewhat with temperature and chemistry), and without a very detailed model of initial contaminant distributions, the performance boost afforded by EO is difficult to quantify. It is reasonable to assume that despite a very small increase in the overall flux of ground water to the extraction wells as a result of EO (most of the water flux is provided by Darcian flow through preferential pathways), the rate of transport through materials with hydraulic conductivities less than 1×10^{-7} cm/s will increase substantially. As a result, low permeability sediments characterized by relatively high concentrations of contaminants in plume source areas would be expected to achieve cleanup objectives in most instances many years or decades ahead of what would be attainable through pump-and-treat operations alone. Cost savings to the project would then be realized through a substantial reduction in the amount of time required to operate and maintain pump-and-treat facilities.

2. Acknowledgments

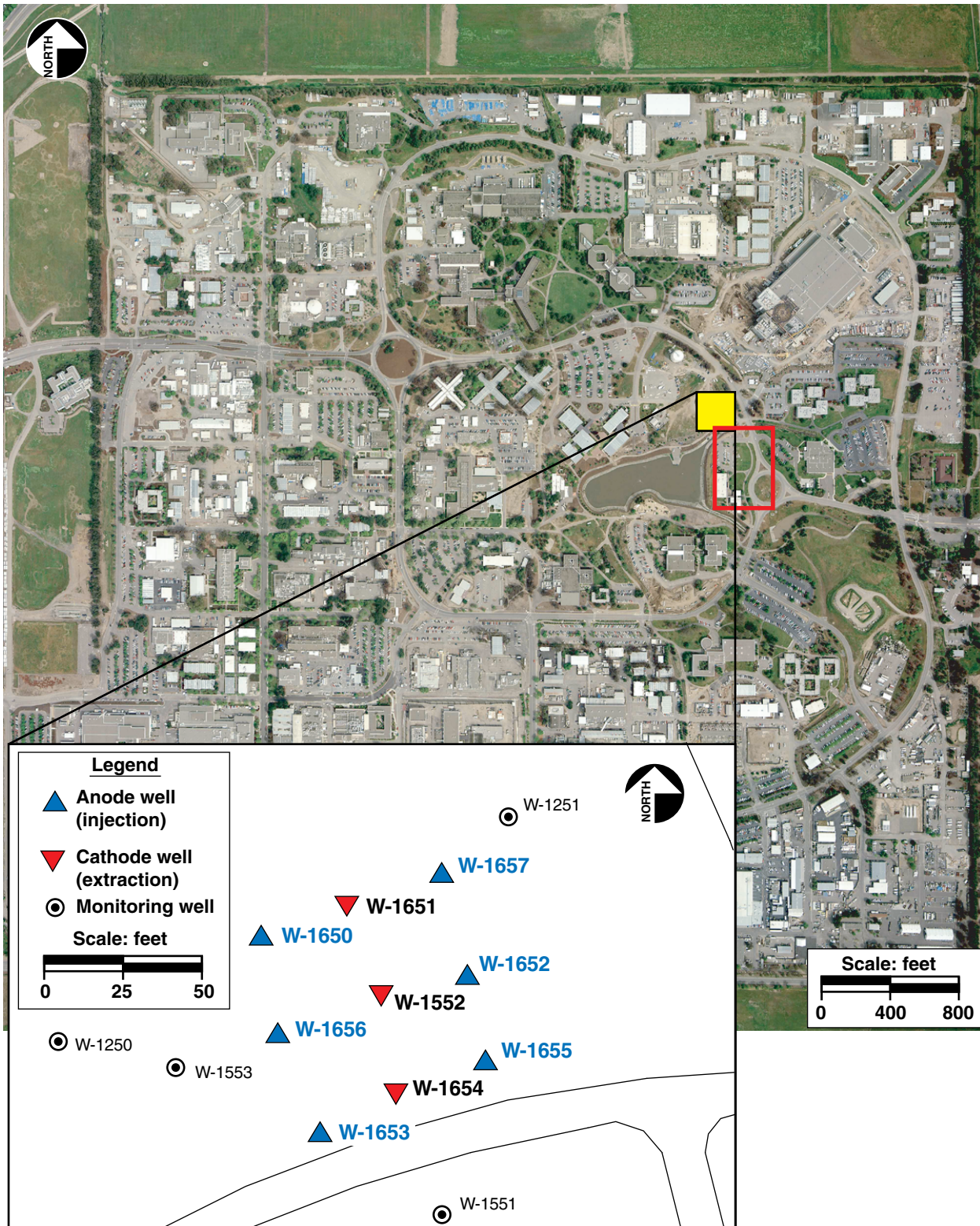
This technology deployment was funded in part by the U.S. DOE's EM-50 program. A number of individuals contributed to the design, construction, and operation of the EO/pump-and-treat system at the Helipad site. These individuals include Allen Elsholz, Dick Hall, Steve Hunter, Ben Johnson, Larry Kita, P.J. Lyra, George Metzger, Tristan Pico, and Herk Van Noy. Zafer Demir provided helpful advice on the interpretation of subsurface hydraulics. Ken Carroll performed analysis of ground water samples for chlorinated hydrocarbons. Geokinetics International, Inc. of Berkeley California supplied equipment and expertise.

3. References

- Acar, Y. B., and A. N. Alshawabkeh (1993), "Principles of Electrokinetic Remediation," *Environ. Sci. and Technol.* **27**(13), 2638–2647.
- Blake, R. G., C. M. Noyes, and M. P. Maley (1995), *Hydrostratigraphic Analysis – The Key to Cost-Effective Ground Water Cleanup at Lawrence Livermore National Laboratory*, Lawrence Livermore National Laboratory, Livermore, Calif. (UCRL-JC-120614).
- Bruell, C. J., B. A. Segall, and M. T. Walsh (1992), "Electroosmotic removal of gasoline hydrocarbons and TCE from clay," *Journal of Environmental Engineering* **118**(1), 68–83.
- Casagrande, I. (1952), *Review of past and current work on electroosmotic stabilization of soils*, Harvard Soil Mechanics Series 38, Supplement 1957.
- Cherepy, N., W. McNab, D. Wildenschild, R. Ruiz, and A. Elsholz (1999), "Electro-osmotic remediation of fine-grained sediments," in *Proceedings of the Electrochemical Society: Environmental Aspects of Electrochemical Technology* (**99**)39, 97–110.
- Gile, L. H., and R. B. Grossman (1979), *The Desert Project Soil Monograph*, Soil Conservation Service, USDA, pp 984.
- Gile, L. H., J. W. Hawley, and R. B. Grossman (1981), *Soils and geomorphology in the Basin and Range area of southern New Mexico – Guidebook to the Desert Project*, New Mexico Bureau of Mines and Mineral Resources Memoir 39, 222 pp.
- Hamed, J., Y. B. Acar, and R. J. Gale (1991), "Pb(II) removal from kaolinite by electrokinetics," *Journal of Geotechnical Engineering*, **117**(2), 241–271.
- Ho, S. V., C. Athmer, and P. W. Sheridan (1999a), "The Lasagna technology for in situ soil remediation. 1: Small field test," *Environ. Sci. and Technol.* **33**(7), 1086–1091.
- Ho, S. V., C. Athmer, and P. W. Sheridan (1999b), "The Lasagna technology for in situ soil remediation. 2: Small field test," *Environ. Sci. and Technol.* **33**(7), 1092–1099.
- Koltermann, C. E., and S. M. Gorelick (1992), "Paleoclimatic signature in terrestrial flood deposits," *Science* **256**, 1775–1782.
- Lageman, R. (1993), "Electroreclamation," *Environ. Sci. and Technol.* **27**(13), 2648–2650.
- McNab, W. W., Jr., and R. Ruiz (2001), "In situ measurement of electro-osmotic fluxes and conductivity using single well-bore tracer tests," *Ground Water Monitoring & Remediation* (UCRL-JC-137440 PREPRINT).
- Mitchell, J. K. (1993), *Fundamentals of Soil Behavior*, 2nd ed. (Wiley, New York), 437 pp.
- Noyes, C. M., M. P. Maley, and R. G. Blake (2000), "Defining Hydrostratigraphic units within the heterogeneous alluvial sediments at Lawrence Livermore National Laboratory," Lawrence Livermore Laboratory, Livermore Calif. (submitted to *Ground Water*).

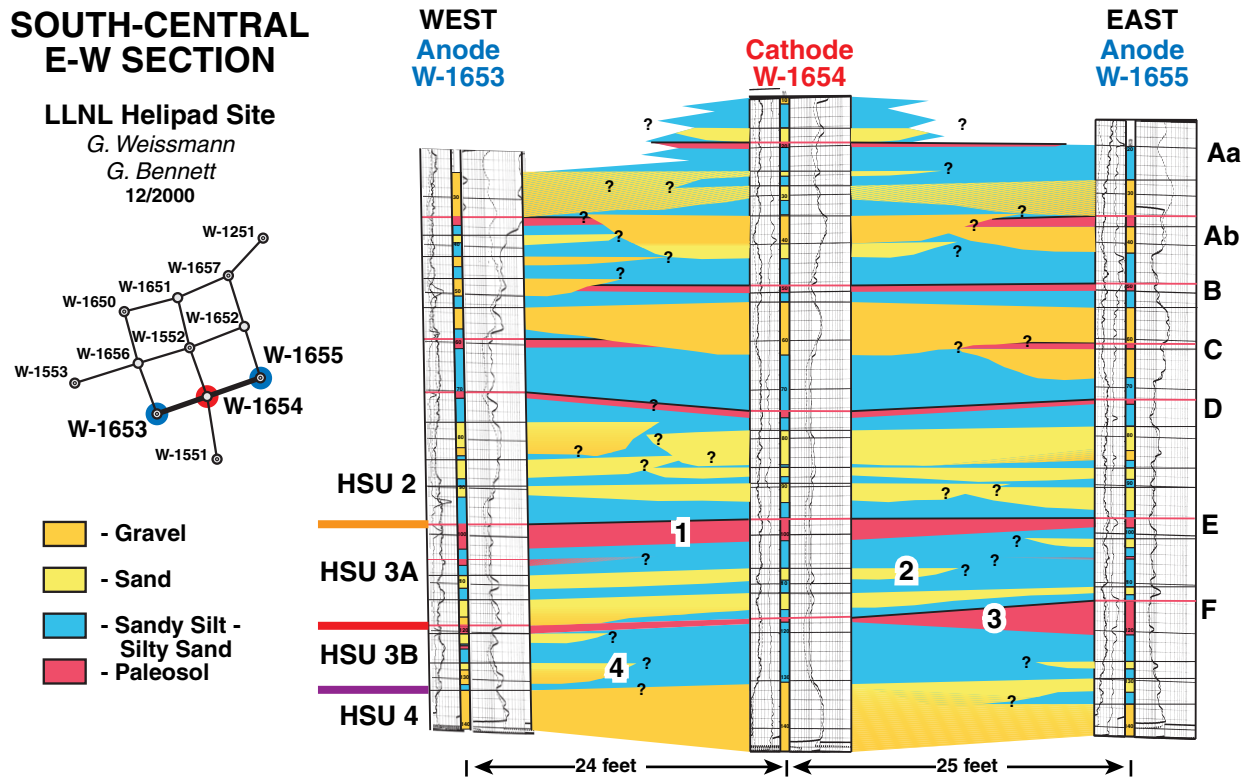
- Pico, T. M. (2000), *Evaluation of Electro-Osmotic-Aided Remediation of Chlorinated Solvent-Contaminated Aquitards - Appendix A, Electroosmotically Aided Restoration of TCE Contaminated Soil*, Final Report to Lawrence Livermore National Laboratory, Livermore, California, by Department of Civil and Environmental Engineering, Lehigh University, Bethlehem, PA (UCRL-ID-137602).
- Probstein, R. F., and R. E. Hicks (1993), "Removal of contaminants from soils by electric fields," *Science* **260**(5107), 498–503.
- Segall, B. A., and C. J. Bruell (1992), "Electroosmotic contaminant removal processes," *Journal of Environmental Engineering* **118**(1), 84–100.
- Shapiro, A. P., and R. F. Probstein (1993), "Removal of contaminants from saturated clay by electroosmosis," *Environ. Sci. and Technol.* **27**(2), 283–291.

Figures



ERD-LSR-01-0084

Figure 1. Aerial photograph of LLNL Livermore Site. Location of the EO field demonstration site (Helipad area) shown in yellow and former East Traffic Circle landfill in red. Detail of EO well field shown in inset.



ERD-LSR-01-0085

Figure 2. An east-west oriented cross section along the southern boundary of the EO deployment site. Numbers 1 and 3 refer to paleosols at HSU 3A and 3B boundaries, respectively. Numbers 2 and 4 illustrate truncation of channel deposits toward the east within HSUs 3A and 3B.



ERD-LSR-01-0086

Figure 3. Photograph of a typical gravel hydrofacies sample. Notice that clasts are well rounded and contain a thick matrix of reddish clay. Additionally, many of these clasts are weathered. The largest clasts are approximately 1 inch (2 to 3 cm) in length.



ERD-LSR-01-0087

Figure 4. Photograph of a typical sand hydrofacies sample.

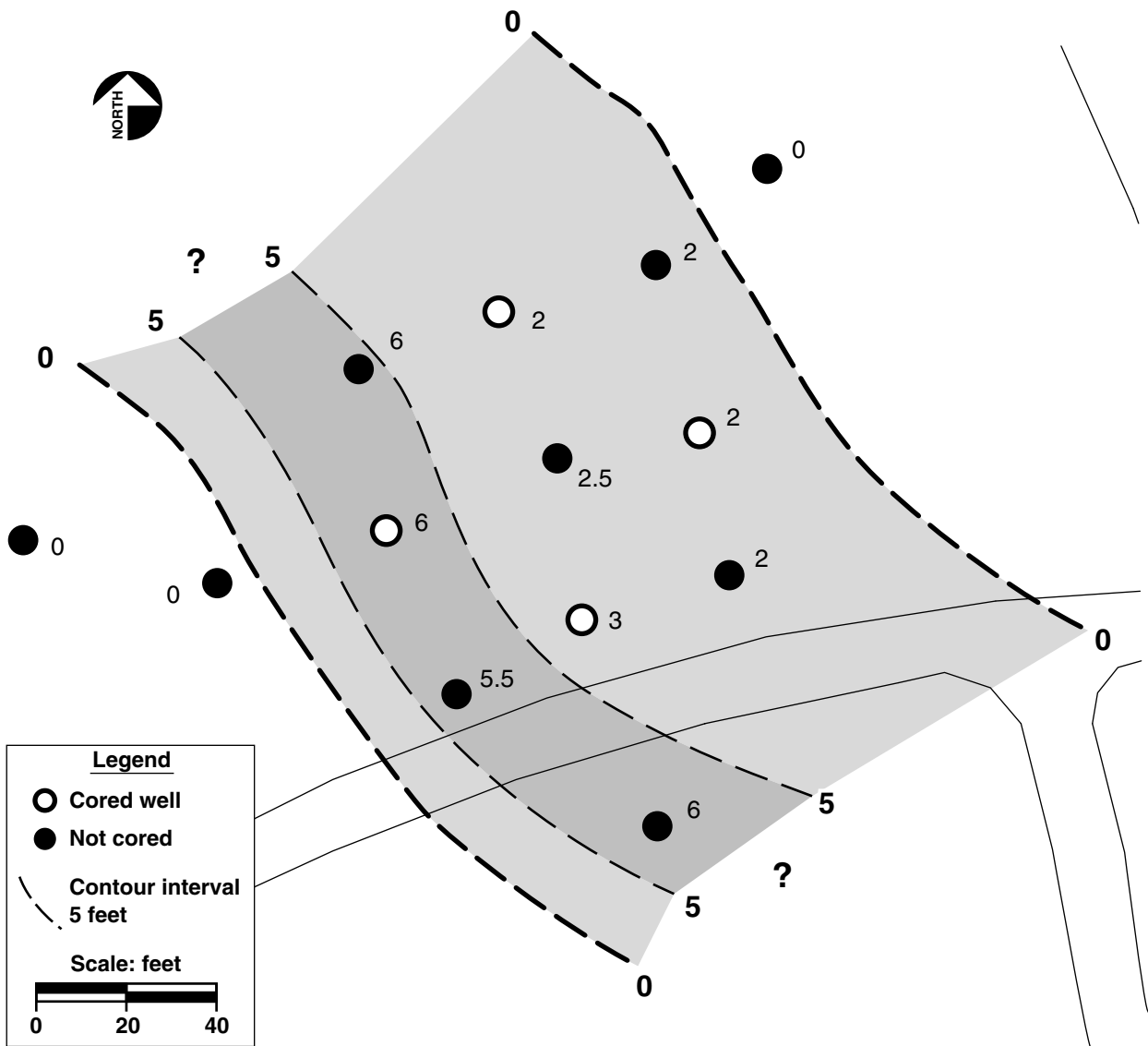


Figure 5. Photograph of a typical sandy silt hydrofacies sample. Note the clay-filled root trace located in the center of this sample (white arrow) and reduction halo around the root trace.



ERD-LSR-01-0088

Figure 6. Photograph of a typical paleosol hydrofacies sample. This image shows two stacked paleosols with different coloration.



ERD-LSR-01-0089

Figure 7. Isopach map of lowest channel deposit within HSU 3A.

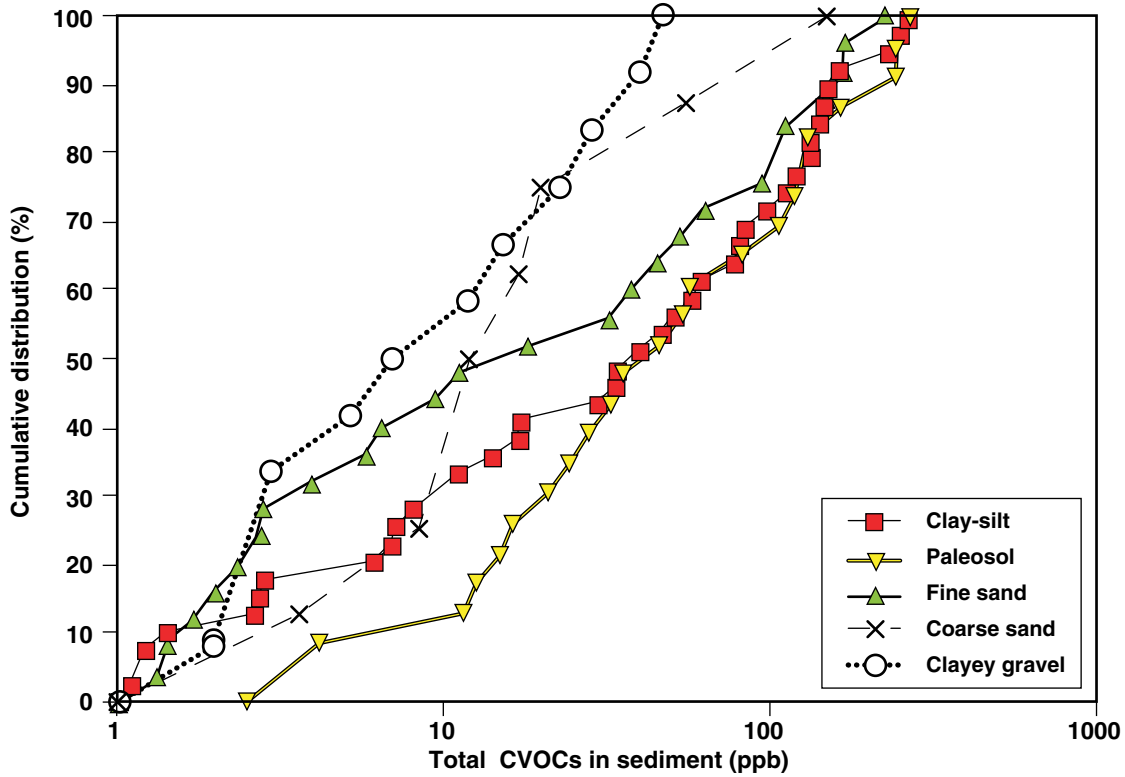
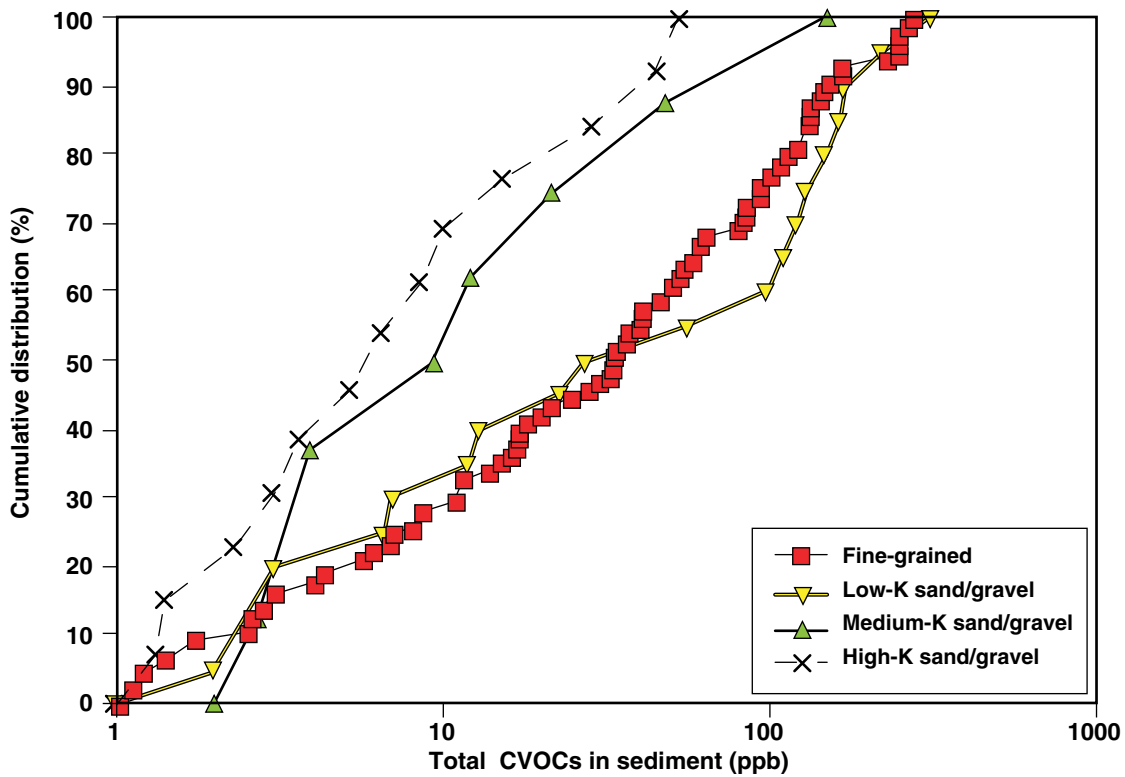
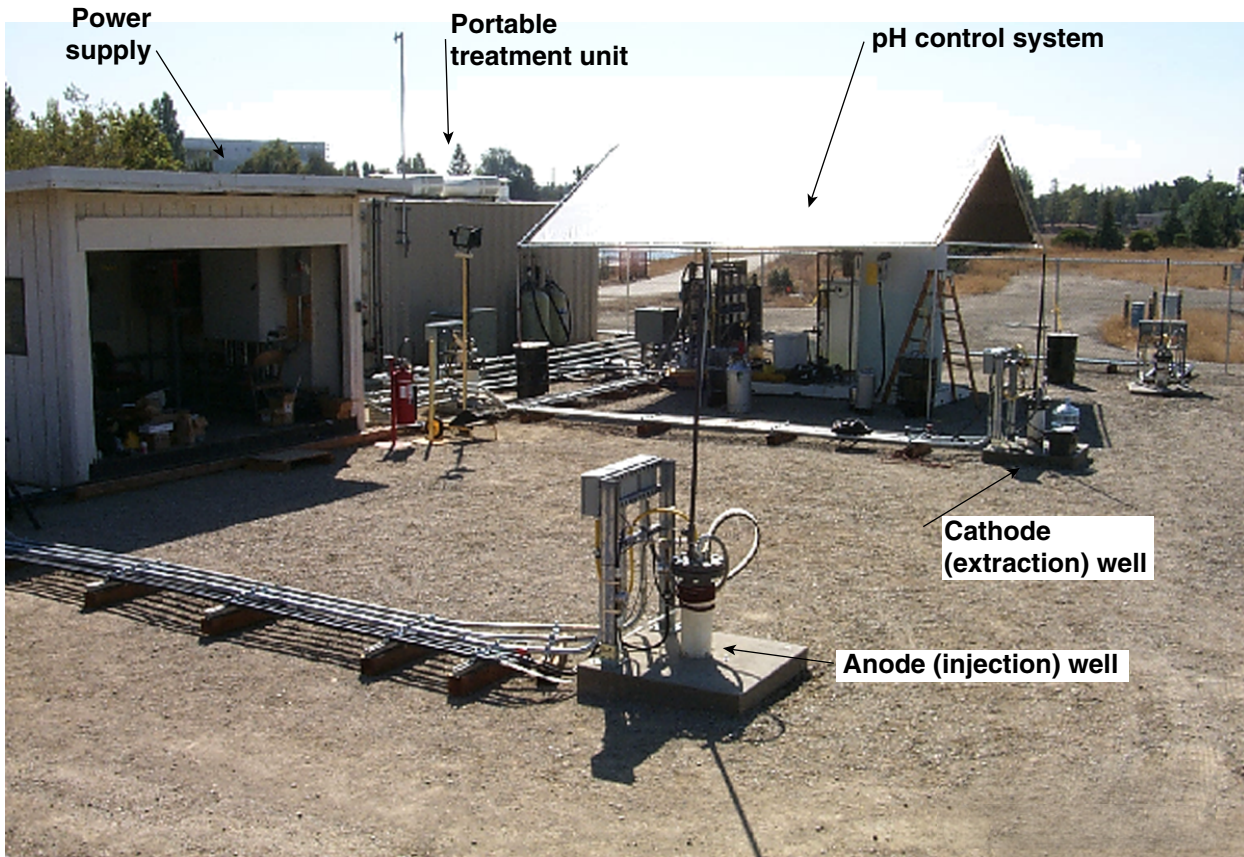
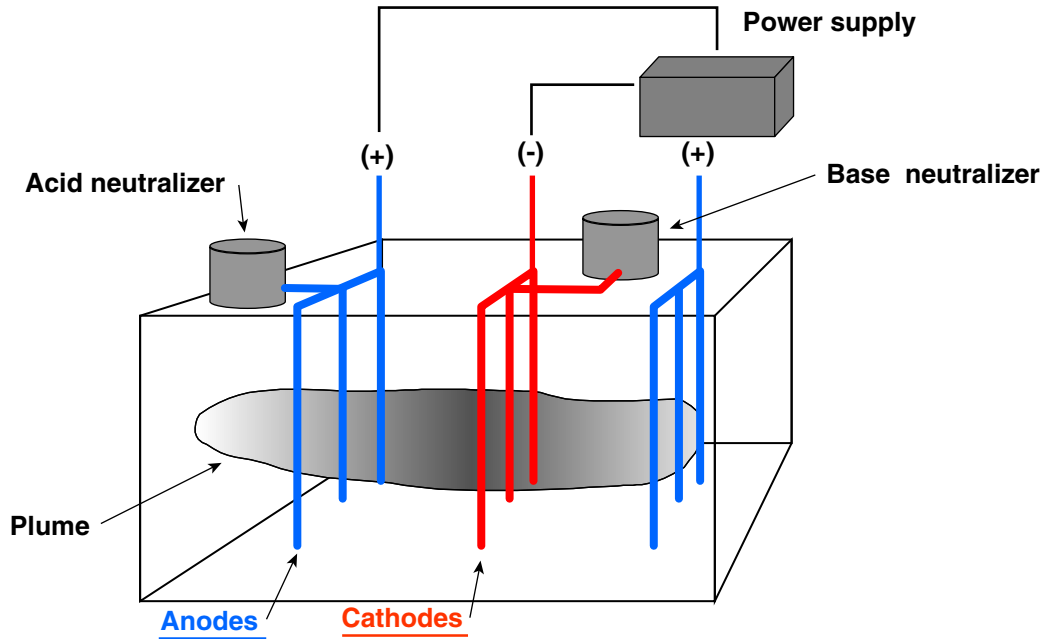


Figure 8a. Sediment total chlorinated hydrocarbon concentrations, grouped by lithologies as delineated by lithologic description of continuous cores.



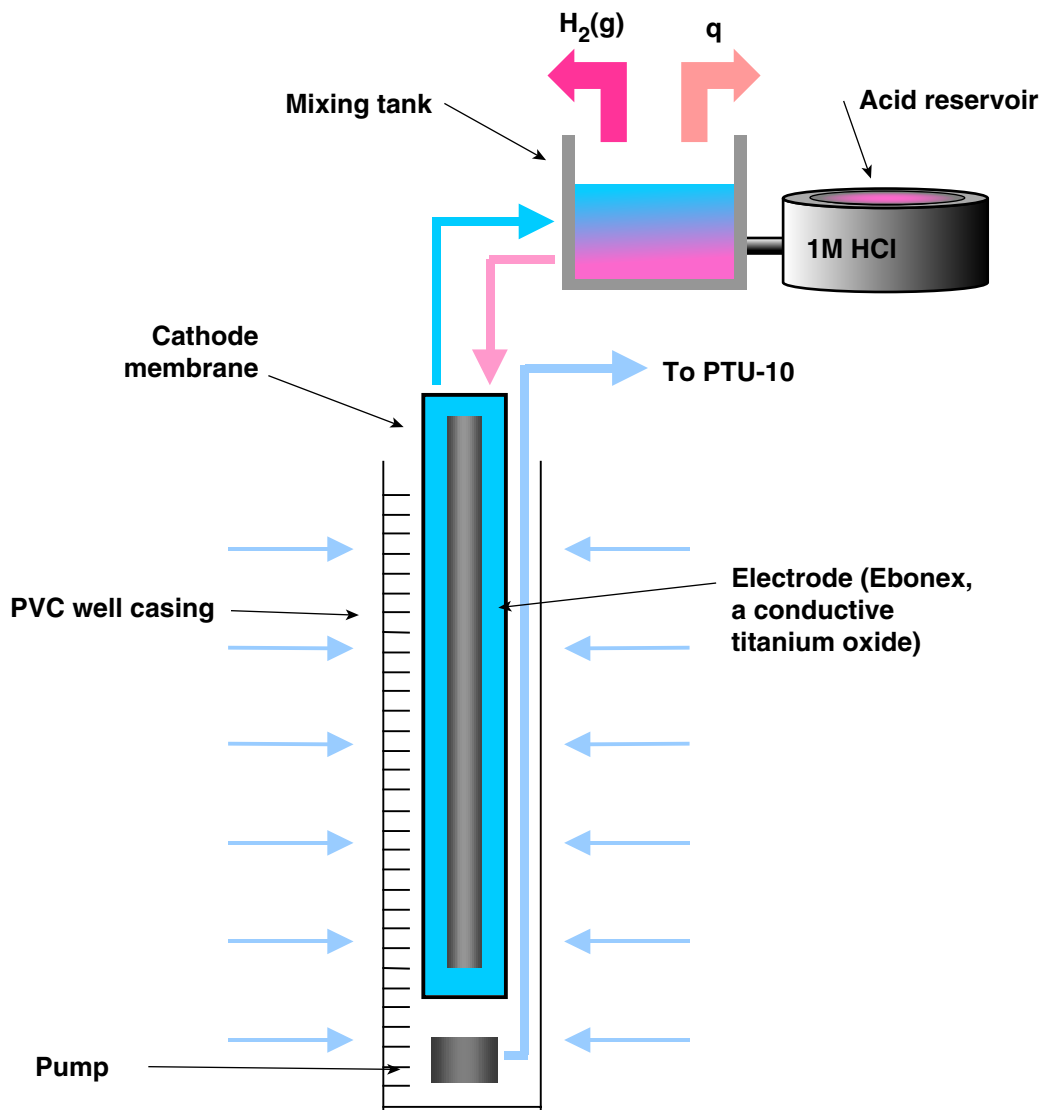
ERD-LSR-01-0090

Figure 8b. Sediment total chlorinated hydrocarbon concentrations concentrations, grouped by lithologies as delineated by geophysical logs.



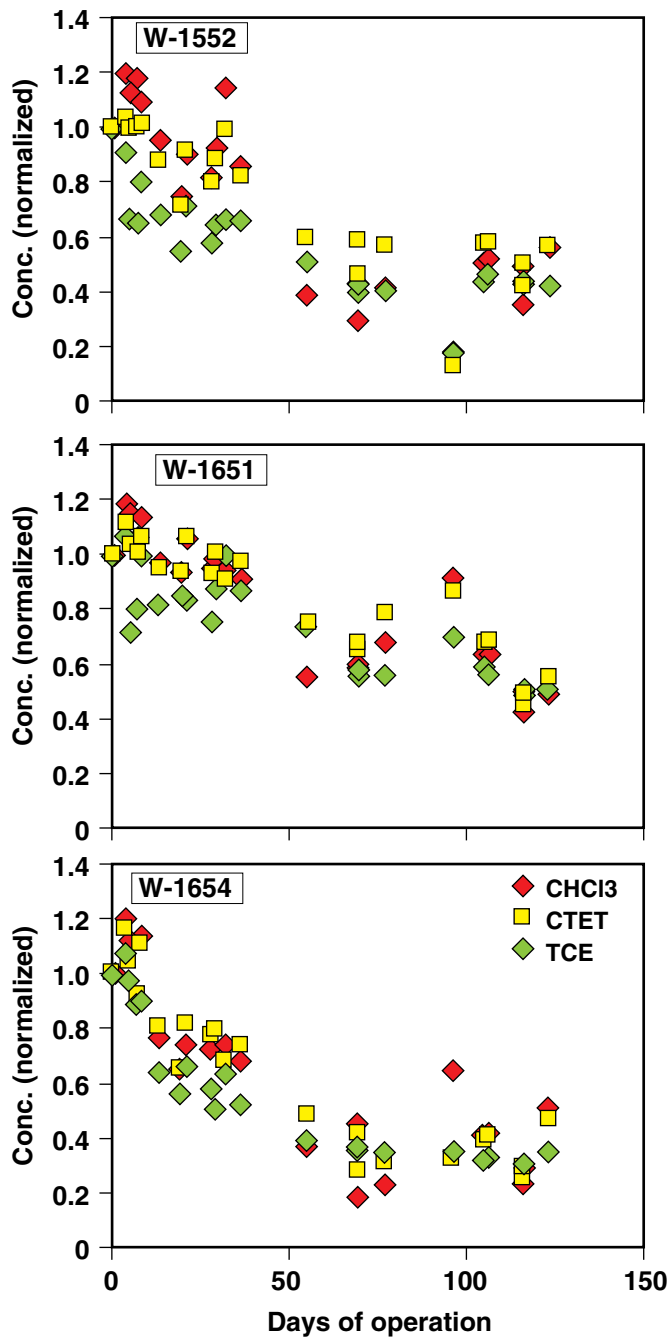
ERD-LSR-01-0091

Figure 9. EO system layout: schematic (top), and photograph of Helipad EO deployment site (bottom).



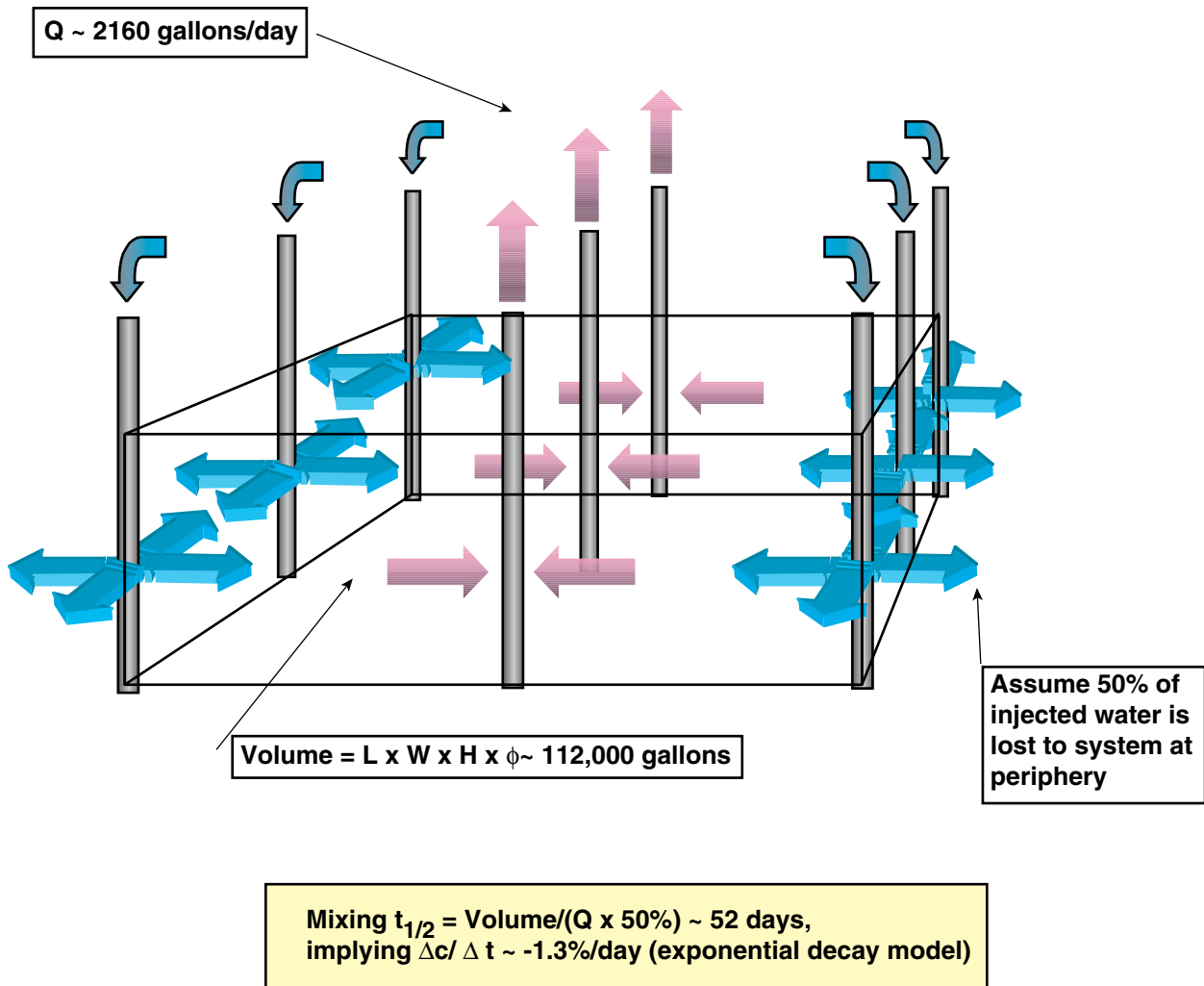
ERD-LSR-01-0092

Figure 10. Cathode membrane assembly.



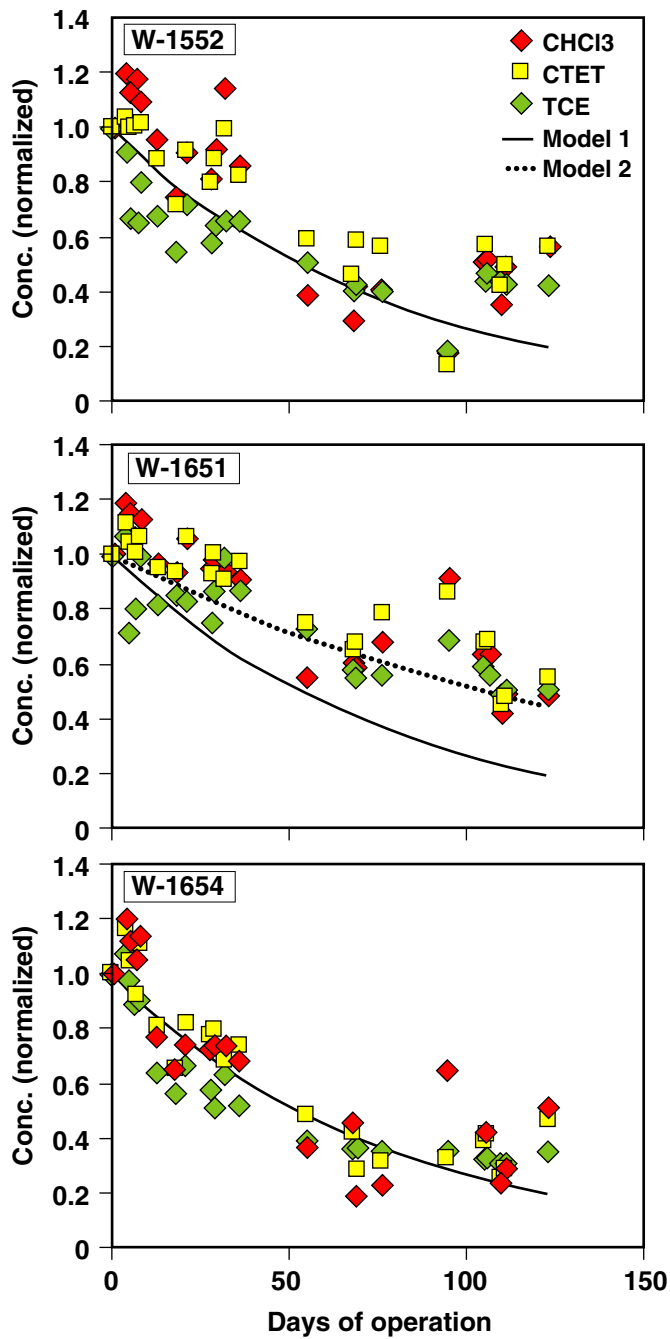
ERD-LSR-01-0093

Figure 11. Chlorinated hydrocarbon concentration histories (concentrations normalized to those measured at the commencement of sampling) for wells W-1552, W-1651, and W-1654.



ERD-LSR-01-0095

Figure 12. An idealized mixed tank model of pump-and-treat with re-injection in Helipad area wells.



ERD-LSR-01-0095

Figure 13. Normalized concentration histories as interpolated by the mixed tank model for wells W-1552, W-1651, and W-1654. “Model” or “Model 1” refer to the mixed tank interpolation model assuming a 50% injection water loss; “Model 2” assumes a 75% loss (i.e., 25% of injected water is retained within system). Model 2 was applied to W-1651 data because that well is suspected to be in hydraulic communication with underlying HSU-4.

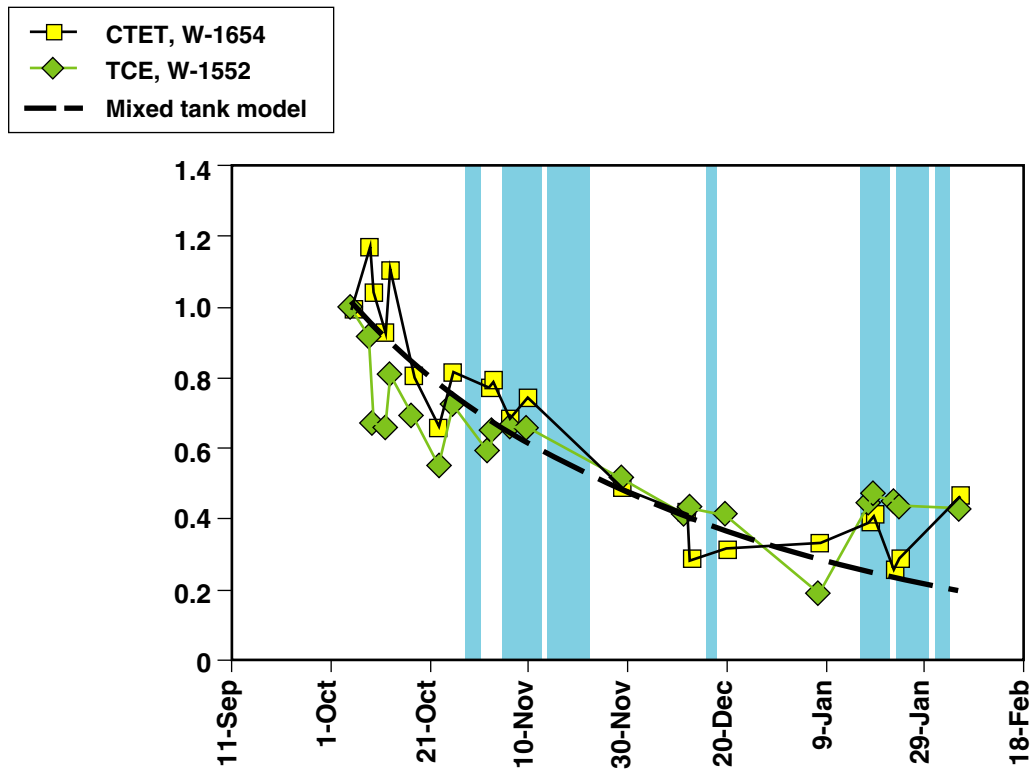
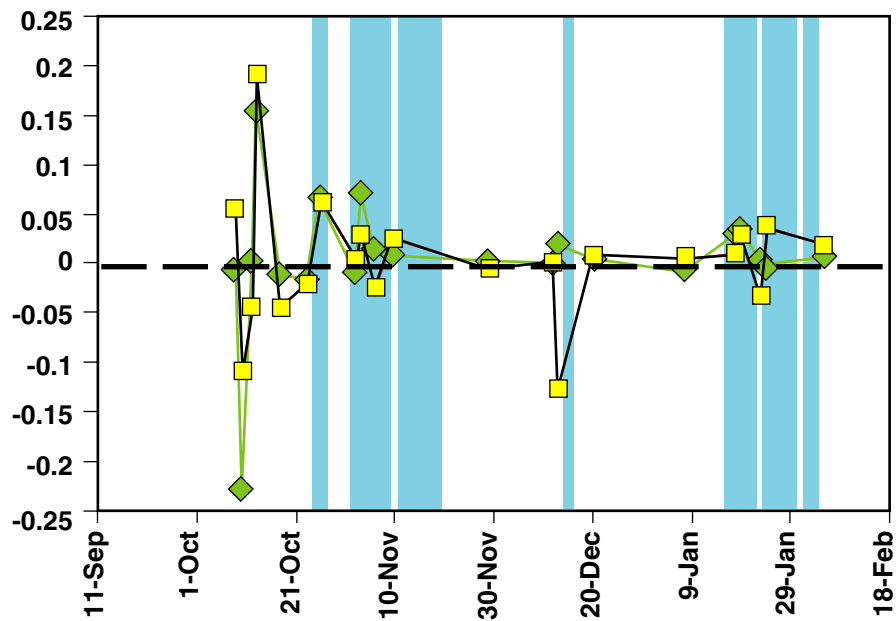
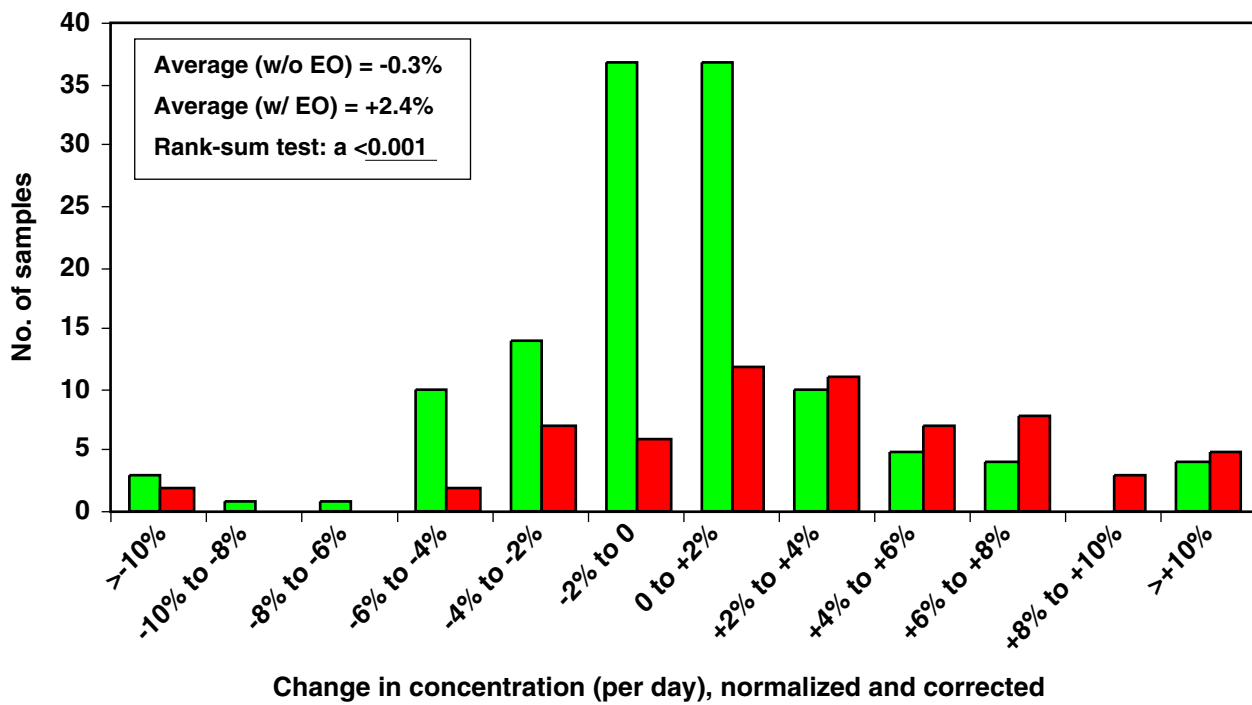


Figure 14a. Normalized concentration histories of TCE in well W-1552 and carbon tetrachloride in well W-1654 (EO operation periods indicated by blue shading).



ERD-LSR-01-0096

Figure 14b. Estimated $\Delta c/\Delta t$ values, corrected by the mixed tank interpolation model. (EO operation periods indicated by blue shading).



ERD-LSR-01-0097

Figure 15. A comparison of frequency distributions of corrected $\Delta c/\Delta t$ values under EO and non-EO operating conditions.

Table

Table 1. $\Delta c/\Delta t$ values for key chlorinated hydrocarbon compounds in each of the three extraction/cathode wells. Changes in normalized concentration are corrected for the effect of pump-and-treat with re-injection. Samples collected during operation of the EO system are indicated in red font with shading.

Date	W-1651			W-1654			W-1552		
	CHCl ₃	CTET	TCE	CHCl ₃	CTET	TCE	CHCl ₃	CTET	TCE
10/05/00	–	–	–	–	–	–	–	–	–
10/09/00	5.30%	3.47%	2.40%	6.25%	5.52%	3.29%	6.22%	2.24%	-0.82%
10/10/00	-3.13%	-5.95%	-34.28%	-5.93%	-10.92%	-8.53%	-5.33%	-3.37%	-22.92%
10/12/00	-3.44%	-1.18%	4.72%	-2.16%	-4.52%	-2.88%	4.15%	2.31%	0.16%
10/13/00	7.23%	6.27%	20.28%	10.02%	19.12%	2.41%	-6.92%	1.83%	15.41%
10/18/00	-2.57%	-1.60%	-2.90%	-5.90%	-4.51%	-4.05%	-1.32%	-1.45%	-1.31%
10/23/00	0.11%	0.39%	1.16%	-1.26%	-2.01%	-0.74%	-3.10%	-2.14%	-1.81%
10/26/00	4.55%	4.94%	-0.18%	3.58%	6.36%	4.08%	6.45%	7.58%	6.47%
11/02/00	-0.82%	-1.31%	-0.51%	0.75%	0.40%	-0.41%	-0.14%	-0.50%	-1.06%
11/03/00	4.36%	8.74%	11.39%	2.54%	2.91%	-5.83%	11.68%	9.89%	6.89%
11/06/00	-0.90%	-2.70%	4.68%	1.01%	-2.71%	4.92%	8.56%	4.74%	1.32%
11/10/00	-0.12%	2.15%	-2.34%	-0.42%	2.35%	-2.06%	-5.71%	-2.90%	0.87%
11/29/00	-1.32%	-0.58%	-0.17%	-0.87%	-0.48%	-0.04%	-1.47%	-0.25%	0.00%
12/12/00	0.76%	-0.23%	-0.68%	1.11%	0.09%	0.20%	-0.21%	-0.26%	-0.17%
12/13/00	-1.43%	3.14%	-2.66%	-26.24%	-12.63%	1.05%	12.82%	12.86%	2.04%
12/20/00	1.69%	1.99%	0.52%	0.89%	0.72%	0.24%	0.36%	0.41%	0.29%
01/08/01	1.67%	0.92%	1.01%	2.45%	0.47%	0.43%	-0.71%	-1.63%	-0.70%
01/18/01	-2.20%	-1.32%	-0.51%	-1.48%	1.00%	0.18%	3.46%	4.57%	2.82%
01/19/01	0.28%	0.88%	-2.70%	0.95%	2.88%	1.09%	1.80%	0.99%	3.29%
01/23/01	-4.92%	-5.39%	-1.46%	-4.05%	-3.37%	-0.16%	-3.44%	-2.92%	0.01%
01/24/01	7.86%	3.93%	1.93%	6.13%	3.70%	0.70%	14.61%	7.81%	-0.26%
02/05/01	0.24%	0.85%	0.36%	2.16%	1.84%	0.76%	1.22%	1.19%	0.47%

Attachment A

Electro-osmosis Screening Model

Attachment A: Electroosmosis Screening Model

This 3-D model is based upon the assumption that the electric field may be defined using simple potential theory. Cathodes and anodes are modeled as electron sources and sinks, respectively, using a continuous point source solution in an infinite homogeneous 3-D domain. Point sources are then integrated in the vertical direction to simulate a continuous line source (i.e. finite length electrode). The groundwater velocity vector field is calculated using an analogy to Darcy's law, where water flow in response to the voltage gradient in a rate proportional to the electroosmotic conductivity coefficient (as measured in the laboratory). This assumes that the hydraulic head distribution is hydrostatic (i.e. there are no driving forces for groundwater flow other than the electric field).

Sediment Properties

$$\sigma_s := 0.05 \frac{\text{S}}{\text{m}} \quad (\text{electric conductivity})$$

$$k_{eo} := 2.3 \cdot 10^{-9} \frac{\text{m}^2}{\text{sec} \cdot \text{V}} \quad (\text{electroosmotic conductivity})$$

$$\eta := 0.30 \quad (\text{porosity})$$

EO System Properties

$$E_L := 20 \text{ ft} \quad (\text{electrode length})$$

$$E_d := 3 \text{ in} \quad r_e := \frac{E_d}{2} \quad (\text{electrode diameter and radius})$$

$$E_A := \pi \cdot r_e \cdot (2 \cdot E_L + r_e) \quad (\text{electrode surface area})$$

Electrode configuration (elevation with reference to bottom of electrode):

N := 4 (total number of electrodes)
 ORIGIN=1 (set first array index = 1)

Geometrical arrangement of electrodes is based on a fence configuration, with a row of anodes facing a row of cathodes.

$$c_e := \begin{bmatrix} 0 \\ 0 \\ -120 \end{bmatrix} \text{ ft} \quad (\text{location of reference cathode})$$

$\Delta x := 25 \text{ ft}$ (east-west spacing)

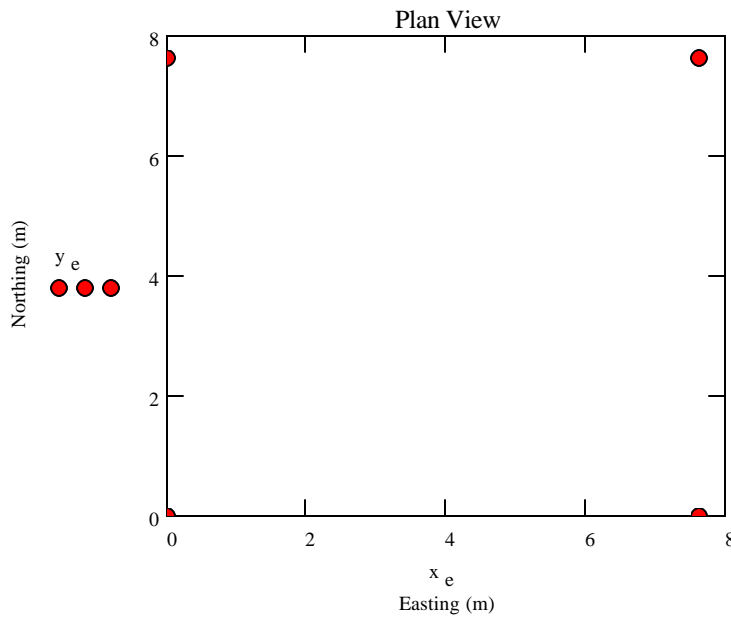
$\Delta y := 25 \text{ ft}$ (north-south spacing)

$$x_e := \begin{bmatrix} c_{e_1} \\ c_{e_1} + \Delta x \\ c_{e_1} \\ c_{e_1} + \Delta x \end{bmatrix}$$

$$y_e := \begin{bmatrix} c_{e_2} \\ c_{e_2} \\ c_{e_2} + \Delta y \\ c_{e_2} + \Delta y \end{bmatrix}$$

$$z_e := \begin{bmatrix} c_{e_3} \\ c_{e_3} \\ c_{e_3} \\ c_{e_3} \end{bmatrix}$$

$$I := \begin{bmatrix} -6 \\ 6 \\ -6 \\ 6 \end{bmatrix} \text{ amp}$$



Potential Field Equations

Distance equation in 3-D:

$$\text{dist3d}(x_1, y_1, z_1, x_2, y_2, z_2) := \sqrt{(x_1 - x_2)^2 + (y_1 - y_2)^2 + (z_1 - z_2)^2}$$

Anode (sink for electrons):

$$\phi(x, y, z) := \sum_{k=1}^N \frac{1}{E_L} \cdot \int_{z_{e_k}}^{z_{e_k} + E_L} \frac{I_k}{4 \cdot \pi \cdot \sigma_s} \cdot \left(\frac{1}{r_e} - \frac{1}{\text{dist3d}(x, y, z, x_{e_k}, y_{e_k}, \zeta)} \right) d\zeta$$

Gradient equations (used to override MathCad routines): $\delta := 1 \text{ cm}$

$$\text{grad}\phi_x(x, y, z) := \frac{(\phi(x + 0.5 \cdot \delta, y, z) - \phi(x - 0.5 \cdot \delta, y, z))}{\delta}$$

$$\text{grad}\phi_y(x, y, z) := \frac{(\phi(x, y + 0.5 \cdot \delta, z) - \phi(x, y - 0.5 \cdot \delta, z))}{\delta}$$

$$\text{grad}\phi_z(x, y, z) := \frac{(\phi(x, y, z + 0.5 \cdot \delta) - \phi(x, y, z - 0.5 \cdot \delta))}{\delta}$$

Induced Groundwater Movement

Groundwater velocity field:

$$v(x, y, z) := \begin{bmatrix} \frac{-k_{eo}}{\eta} \cdot \text{grad}\phi_x(x, y, z) \\ \frac{-k_{eo}}{\eta} \cdot \text{grad}\phi_y(x, y, z) \\ \frac{-k_{eo}}{\eta} \cdot \text{grad}\phi_z(x, y, z) \end{bmatrix}$$

Volumetric flux of water to the first cathode:

(1) Define a function describing the normal vector to a vertical cylinder surrounding the cathode.

$$\text{cndr}(x, y, z) := \begin{bmatrix} x - x_{e_1} \\ y - y_{e_1} \\ 0 \end{bmatrix} \quad n(x, y, z) := \frac{\text{cndr}(x, y, z)}{\sqrt{\text{cndr}(x, y, z) \cdot \text{cndr}(x, y, z)}}$$

(2) Find component of groundwater velocity vector normal to cylinder (dot product).

$$v_n(x, y, z) := v(x, y, z) \cdot n(x, y, z)$$

(3) Evaluate surface integral about encompassing cylinder.

$$\rho := 2 \text{ ft} \quad (\text{radius of cylinder encompassing cathode})$$

$$Q_{EO} := E_L \cdot \int_0^{2\pi} -\eta \cdot v_n \left(x_{e_1} + \rho \cdot \cos(\theta), y_{e_1} + \rho \cdot \sin(\theta), z_{e_1} + \frac{E_L}{2} \right) \cdot \rho \, d\theta$$

$$|Q_{EO}| = 16.26 \frac{\text{cm}^3}{\text{min}}$$

$$\frac{|Q_{EO}|}{0.5 \frac{\text{gal}}{\text{min}}} = 0.859 \%$$

Note that this analysis neglects (1) vertical variations in flux along the cylinder, and (2) flux contributions through the ends of the cylinder.

Particle Travel Time

Time step size: $\Delta t := 200 \text{ day}$ Number of time steps: $n_t := 59$

End time: $t_f := n_t \cdot \Delta t$ $t_f = 32.307 \cdot \text{yr}$

Explicit finite-difference approximation for particle migration over Δt : $\text{iter} := 1.. n_t$

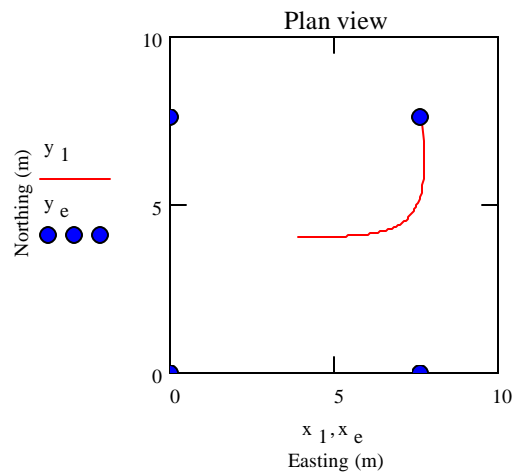
Initial conditions:

$$\begin{bmatrix} t_1 \\ x_{1_{\text{iter}}} \\ y_{1_{\text{iter}}} \\ z_{1_{\text{iter}}} \end{bmatrix} := \begin{bmatrix} 0 \text{ day} \\ x_{e_1} + 0.51 \cdot \Delta x \\ y_{e_1} + 0.49 \cdot \Delta y + 1 \text{ ft} \\ z_{e_1} + 0.5 \cdot E_L \end{bmatrix}$$

Finite difference solution:

$$\begin{bmatrix} t_{\text{iter}+1} \\ x_{1_{\text{iter}+1}} \\ y_{1_{\text{iter}+1}} \\ z_{1_{\text{iter}+1}} \end{bmatrix} := \begin{bmatrix} t_{\text{iter}} + \Delta t \\ x_{1_{\text{iter}}} + \Delta t \cdot v(x_{1_{\text{iter}}}, y_{1_{\text{iter}}}, z_{1_{\text{iter}}})_1 \\ y_{1_{\text{iter}}} + \Delta t \cdot v(x_{1_{\text{iter}}}, y_{1_{\text{iter}}}, z_{1_{\text{iter}}})_2 \\ z_{1_{\text{iter}}} + \Delta t \cdot v(x_{1_{\text{iter}}}, y_{1_{\text{iter}}}, z_{1_{\text{iter}}})_3 \end{bmatrix}$$

Effective mean velocity:
$$\frac{\text{dist3d}(x_{1_1}, y_{1_1}, z_{1_1}, x_{1_{n_t}}, y_{1_{n_t}}, z_{1_{n_t}})}{t_{n_t} - t_1} = 1.357 \cdot 10^{-3} \frac{\text{ft}}{\text{day}}$$



Operational Summary

Potential difference across example anode-cathode set:

$$\Delta V := \phi \left(x_{e_2} - 1 \text{ cm}, y_{e_2}, z_{e_2} + 0.5 \cdot E_L \right) - \phi \left(x_{e_1} + 1 \text{ cm}, y_{e_1}, z_{e_1} + 0.5 \cdot E_L \right)$$

$$\Delta V = -38.433 \text{ V}$$

Per electrode pair power consumption:

$$P := I_1 \cdot \Delta V$$

$$P = 0.231 \text{ kW}$$

Attachment B
Pumping Model in 3-D

Attachment B:Pumping Model in 3-D

This 3-D model is based upon point sources and sinks for water within a homogeneous, infinite 3-D aquifer. Point sources are converted to line sources by integrating in the vertical direction.

Aquifer Properties

$$K := 1 \cdot 10^{-7} \frac{\text{cm}}{\text{sec}} \quad (\text{hydraulic conductivity - silt})$$

$$\eta := 0.30 \quad (\text{porosity})$$

Coupled Extraction/injection Well System

$$r_w := 3 \text{ in} \quad (\text{pumping well radius})$$

$$S_L := 20 \text{ ft} \quad (\text{length of screened interval})$$

Electrode configuration (elevation with reference to bottom of well screen):

$$N := 4 \quad (\text{total number of wells})$$

$$\text{ORIGIN} := 1 \quad (\text{set first array index} = 1)$$

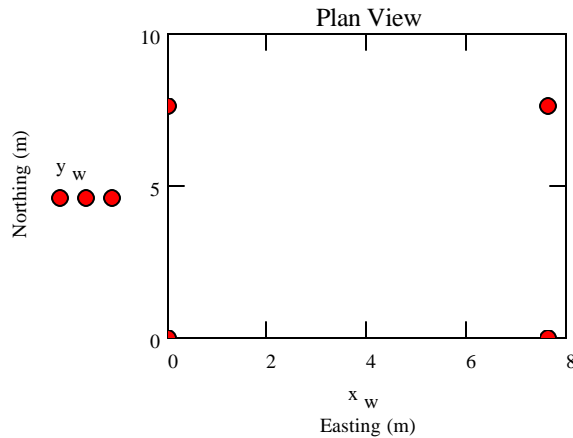
Geometrical arrangement of wells is based on a fence configuration, with a row of injection wells facing a row of extraction wells.

$$c_w := \begin{bmatrix} 0 \\ 0 \\ -120 \end{bmatrix} \text{ ft} \quad (\text{location of reference well})$$

$$\Delta x := 25 \text{ ft} \quad (\text{east-west spacing})$$

$$\Delta y := 25 \text{ ft} \quad (\text{north-south spacing})$$

$$x_w := \begin{bmatrix} c_{w_1} \\ c_{w_1} + \Delta x \\ c_{w_1} \\ c_{w_1} + \Delta x \end{bmatrix} \quad y_w := \begin{bmatrix} c_{w_2} \\ c_{w_2} \\ c_{w_2} + \Delta y \\ c_{w_2} + \Delta y \end{bmatrix} \quad z_w := \begin{bmatrix} c_{w_3} \\ c_{w_3} \\ c_{w_3} \\ c_{w_3} \end{bmatrix} \quad Q := \begin{bmatrix} -0.001 \\ 0.001 \\ -0.001 \\ 0.001 \end{bmatrix} \frac{\text{gal}}{\text{min}}$$



Potential Field Equations

Distance equation in 3-D:

$$\text{dist3d}(x_1, y_1, z_1, x_2, y_2, z_2) := \sqrt{(x_1 - x_2)^2 + (y_1 - y_2)^2 + (z_1 - z_2)^2}$$

Hydraulic potential (negative sign for Q needed to offset negative integration limits):

$$\phi(x, y, z) := \sum_{l=1}^N \frac{1}{S_L} \cdot \int_{z_{w_l}}^{z_{w_l} + S_L} \frac{Q_l}{4 \cdot \pi \cdot K} \left(\frac{1}{r_w} - \frac{1}{\text{dist3d}(x, y, z, x_{w_l}, y_{w_l}, \zeta)} \right) d\zeta$$

Gradient equations (used to override MathCad routines): $\delta := 1 \text{ cm}$

$$\text{grad}\phi_x(x, y, z) := \frac{(\phi(x + 0.5 \cdot \delta, y, z) - \phi(x - 0.5 \cdot \delta, y, z))}{\delta}$$

$$\text{grad}\phi_y(x, y, z) := \frac{(\phi(x, y + 0.5 \cdot \delta, z) - \phi(x, y - 0.5 \cdot \delta, z))}{\delta}$$

$$\text{grad}\phi_z(x, y, z) := \frac{(\phi(x, y, z + 0.5 \cdot \delta) - \phi(x, y, z - 0.5 \cdot \delta))}{\delta}$$

Induced Groundwater Movement

Groundwater velocity field:

$$v(x, y, z) := \begin{bmatrix} \frac{-K}{\eta} \cdot \text{grad}\phi_x(x, y, z) \\ \frac{-K}{\eta} \cdot \text{grad}\phi_y(x, y, z) \\ \frac{-K}{\eta} \cdot \text{grad}\phi_z(x, y, z) \end{bmatrix}$$

Particle Travel Time

Time step size: $\Delta t := 2000 \text{ day}$ Number of time steps: $n_t := 27$

End time: $t_f := n_t \cdot \Delta t$ $t_f = 147.847 \cdot \text{yr}$

Explicit finite-difference approximation for particle migration over Δt : $\text{iter} := 1.. n_t$

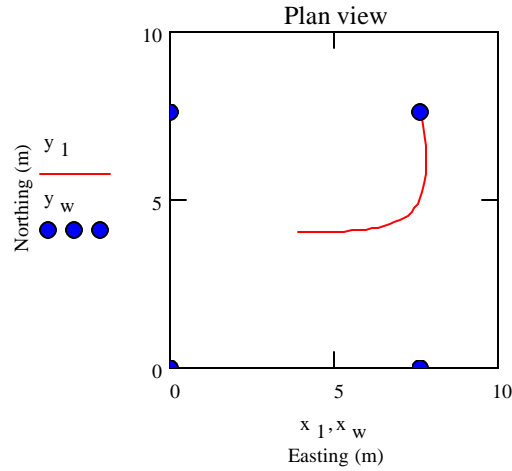
Initial conditions:

$$\begin{bmatrix} t_1 \\ x_{1_{\text{iter}}} \\ y_{1_{\text{iter}}} \\ z_{1_{\text{iter}}} \end{bmatrix} := \begin{bmatrix} 0 \text{ day} \\ x_{w_1} + 0.51 \cdot \Delta x \\ y_{w_1} + 0.49 \cdot \Delta y + 1 \text{ ft} \\ z_{w_1} + 0.5 \cdot S_L \end{bmatrix}$$

Finite difference solution:

$$\begin{bmatrix} t_{\text{iter}+1} \\ x_{1_{\text{iter}+1}} \\ y_{1_{\text{iter}+1}} \\ z_{1_{\text{iter}+1}} \end{bmatrix} := \begin{bmatrix} t_{\text{iter}} + \Delta t \\ x_{1_{\text{iter}}} + \Delta t \cdot v(x_{1_{\text{iter}}}, y_{1_{\text{iter}}}, z_{1_{\text{iter}}})_1 \\ y_{1_{\text{iter}}} + \Delta t \cdot v(x_{1_{\text{iter}}}, y_{1_{\text{iter}}}, z_{1_{\text{iter}}})_2 \\ z_{1_{\text{iter}}} + \Delta t \cdot v(x_{1_{\text{iter}}}, y_{1_{\text{iter}}}, z_{1_{\text{iter}}})_3 \end{bmatrix}$$

Effective mean velocity:
$$\frac{\text{dist3d}(x_{1_1}, y_{1_1}, z_{1_1}, x_{1_{n_t}}, y_{1_{n_t}}, z_{1_{n_t}})}{t_{n_t} - t_1} = 2.956 \cdot 10^{-4} \frac{\text{ft}}{\text{day}}$$



Required Head Differences Between Extraction and Injection Well Pair

$$\Delta h := \phi(x_{w_2} - 1 \text{ cm}, y_{w_2}, z_{w_2} + 0.5 \cdot S_L) - \phi(x_{w_1} + 1 \text{ cm}, y_{w_1}, z_{w_1} + 0.5 \cdot S_L)$$

$\Delta h = -66.287 \text{ ft}$